Inorganic Chemistry

Article

pubs.acs.org/IC

New Layered-Type Quaternary Chalcogenides, Tl_2PbMQ_4 (M = Zr, Hf; Q = S, Se): Structure, Electronic Structure, and Electrical Transport Properties

Cheriyedath Raj Sankar, Abdeljalil Assoud, and Holger Kleinke*

Department of Chemistry and Waterloo Institute for Nanotechnology, University of Waterloo, Waterloo, Ontario, Canada N2L 3G1

Supporting Information

ABSTRACT: We have synthesized and characterized new thallium chalcogenides of the general formula Tl_2PbMQ_4 (M = Zr, Hf; Q = S, Se) from the constituent elements via high-temperature reaction conditions. These sulfides and selenides crystallize in the monoclinic crystal system (space group $C2/c$). The unit cell parameters refined from single-crystal X-ray diffraction data for Tl_2PbZrS_4 are a = 15.455(4) Å, b = 8.214(2) Å, c = 6.751(2) Å, β = 109.093(3)°, and V = 809.9(4) Å^3, with Z = 4. No corresponding tellurides were obtained from similar reaction conditions. The isostructural quaternary chalcogenides form a layered structure, composed of alternating metal and chalcogen layers. The latter are packed along the a axis as in the face-centered cubic packing (ABC), while the metal layers alternate between Tl layers and mixed Pb/Zr layers. All metal atoms are located in differently distorted Q_6 octahedra, with the TlQ_6 polyhedra being the least regular ones. Density functional theory based electronic structure calculations with inclusion of relativistic spin−orbit interactions predict (indirect) energy band gaps of 0.66 and 0.33 eV for Tl_2PbZrS_4 and $Tl_2PbHfSe_4$, respectively. Optical spectroscopy revealed significantly larger (direct) band gaps of 1.2 and 1.6 eV. The semiconducting character is in agreement with the charge-balanced formula $(Tl^+)_2Pb^{2+}M^{4+}(Q^{2-})_4$. The electrical transport properties also show the semiconducting nature of these materials. For $Tl_2PbHfSe_4$, the Seebeck coefficient increases from +190 μV K^{-1} at room temperature to +420 μV K^{-1} at 520 K.

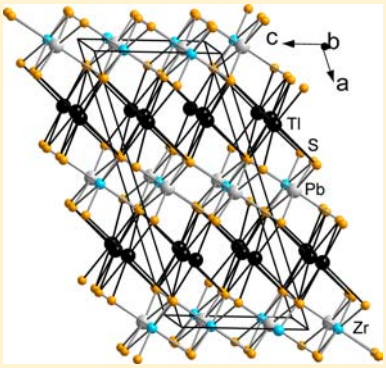

INTRODUCTION

With an increased recent attention to energy conversion and alternate energy sources, inorganic compound semiconductors have found their place in the frontiers of energy materials research. An important such application is in the thermoelectric energy conversion, where the focus lies on heavily doped heavy metal chalcogenides.[1−4] In thermoelectrics, one of the important criteria is that the thermal conductivity of the material should be as low as possible. This can be easily concluded from the equation for the thermoelectric figure of merit, $ZT = TS^2\sigma/\kappa$, where S is the Seebeck coefficient, σ the electrical conductivity, and κ the thermal conductivity at a temperature T. Nanostructuring and optimizing the processing conditions have also been important strategies to bring down the thermal conductivity of materials and possibly enhance the Seebeck coefficient. These strategies have been found to be effective in improving the efficiency of such materials (devices) to a large extent.[5−8]

In thermoelectrics, Tl-based compounds are attractive due to the following reasons: (a) Tl being a heavy metal, it helps reducing the lattice thermal conductivity, and (b) it helps in creating a complex coordination environment around it due to the presence of a lone pair of electrons. These effects are very apparent in promising thermoelectrics, such as Tl_9SbTe_6,[9] Tl_9BiTe_6,[10] $Tl_{10-x}Sn_xTe_6$,[11] $TlBiTe_2$,[12] $TlSbTe_2$,[13] and $TlAg_9Te_5$.[14] To utilize these characteristics, we began recently to explore Tl-based ternary and quaternary chalcogenides incorporating a group 4 metal atom. During this process, we successfully determined the structures and physical properties of Tl_2MQ_3[15,16] and Tl_4MQ_4[17,18], with M = Zr, Hf and Q = S, Se, and Te, with maximum ZT values of undoped, cold-pressed materials of the order of 0.1−0.2. In each case, the sulfides and selenides are isostructural, while the tellurides form different, to date unique, structure types. Most recently, we discovered another new, very complex material by adding a late p-group metal from group 14 into the synthesis, namely, Pb: the chalcogenides $Tl_{18}Pb_2M_7Q_{25}$ (with M = Ti, Zr, Hf and Q = S, Se) are semiconductors with experimentally determined band gaps between 0.1 and 0.5 eV.[19] In this contribution, we report a new class of quaternary compounds with the general formula Tl_2PbMQ_4 (M = Zr, Hf and Q = S, Se), which adopts another new structure type. To date, we were unable to prepare an analogous telluride.

EXPERIMENTAL SECTION

Syntheses and Phase Purity Analyses. The target compositions were synthesized from the constituent elements stored in an argon-filled glovebox (Tl granules, 99.9% (Alfa Aesar); Pb powder (99.9%, Alfa Aesar); Zr pieces, 98.5% (Alfa Aesar); Hf powder −100 mesh,

Received: May 15, 2013
Published: November 21, 2013

   dx.doi.org/10.1021/ic4025316 | Inorg. Chem. 2013, 52, 13869−13874

Table 1. Crystallographic Details of Tl_2PbZrS_4, $Tl_2PbZrSe_4$, Tl_2PbHfS_4, and $Tl_2PbHfSe_4$

	Tl_2PbZrS_4	$Tl_2PbZrSe_4$	Tl_2PbHfS_4	$Tl_2PbHfSe_4$
T of measurement [K]	296(2)	296(2)	296(2)	296(2)
wavelength [Å]	0.71073	0.71073	0.71073	0.71073
crystal system	monoclinic	monoclinic	monoclinic	monoclinic
space group	$C2/c$	$C2/c$	$C2/c$	$C2/c$
a [Å]	15.455(4)	15.906(3)	15.470(2)	15.9480(6)
b [Å]	8.214(2)	8.472(1)	8.226(1)	8.4720(3)
c [Å]	6.751(2)	7.016(1)	6.7103(7)	6.9733(2)
β [deg]	109.093(3)	109.014(2)	109.265(8)	109.121(2)
V [Å^3]	809.9(4)	893.8(2)	806.0(2)	890.19(5)
Z	4	4	4	4
ρ_{calcd} [g/cm^3]	6.851	7.602	7.603	8.284
$R1/wR2$ ($I > 2\sigma$ (I))[a]	0.041/0.075	0.047/0.096	0.043/0.072	0.017/0.042

[a] $R1 = \sum||F_o| - |F_c||/\sum|F_o|$; $wR2 = [\sum[w(F_o^2 - F_c^2)^2]/\sum[w(F_o^2)^2]]^{1/2}$.

Table 2. Atomic Positions of Tl_2PbZrS_4, $Tl_2PbZrSe_4$, Tl_2PbHfS_4, and $Tl_2PbHfSe_4$

atom	Wyckoff site	x	y	z	U_{eq}/Å^2
			Tl_2PbZrS_4		
Tl	8f	0.24920(4)	0.37461(9)	0.23229(8)	0.0277(2)
Pb	4e	0	0.6239(1)	1/4	0.0211(2)
Zr	4e	0	0.1226(2)	1/4	0.0116(3)
S1	8f	0.0966(2)	0.1042(4)	0.0016(4)	0.0159(7)
S2	8f	0.1066(3)	0.3391(4)	0.4641(5)	0.0208(8)
			$Tl_2PbZrSe_4$		
Tl	8f	0.24823(4)	0.37420(9)	0.22966(9)	0.0274(2)
Pb	4e	0	0.6229(1)	1/4	0.0217(2)
Zr	4e	0	0.1238(2)	1/4	0.0133(4)
Se1	8f	0.09988(9)	0.1045(2)	0.0032(2)	0.0146(3)
Se2	8f	0.1089(1)	0.3444(2)	0.4679(2)	0.0172(3)
			Tl_2PbHfS_4		
Tl	8f	0.24923(5)	0.37448(9)	0.23053(7)	0.0244(2)
Pb	4e	0	0.62321(9)	1/4	0.0172(2)
Hf	4e	0	0.12089(9)	1/4	0.0114(2)
S1	8f	0.0958(2)	0.1019(3)	0.0028(4)	0.0112(5)
S2	8f	0.1069(3)	0.3365(3)	0.4638(4)	0.0126(6)
			$Tl_2PbHfSe_4$		
Tl	8f	0.24810(1)	0.37401(2)	0.22859(4)	0.0230(1)
Pb	4e	0	0.62245(3)	1/4	0.0164(1)
Hf	4e	0	0.12311(3)	1/4	0.0103(1)
Se1	8f	0.09872(3)	0.10301(5)	0.00356(7)	0.0102(1)
Se2	8f	0.10873(3)	0.34230(6)	0.46690(7)	0.0126(1)

99.6% (Alfa Aesar); S flakes, 99.98% (Aldrich); and Se pellets, 99.9% (Alfa Aesar)). The elements Tl and Pb were purified prior to use. The elements were loaded in the required stoichiometry into quartz ampules and sealed under vacuum. These ampules were heated slowly to 1073 K in a resistance furnace, allowed to remain at 1073 K for 100 h, and cooled down to 673 K at a rate of 2 K/h, and finally, the furnace was switched off to cool down to room temperature. All tubes contained microcrystalline powder, from which single crystals were successfully extracted for the structure determinations. Both sulfides appeared to be dark brown, and the selenides black.

For phase purity analysis, powder X-ray diffraction experiments of the samples were performed using an INEL powder diffractometer with a position-sensitive detector and Cu-Kα_1 radiation. As shown in the Supporting Information, the respective target phases were obtained in high yields. Energy-dispersive analysis of X-rays was performed on selected crystals of the nominal composition Tl_2PbHfS_4 using an electron microscope with an additional EDX device (Zeiss Ultra SEM/EDAX Team). The sample was bombarded with an acceleration voltage of 20 kV under high dynamic vacuum. No heteroelements, such as Si from the reaction container, were detected. The obtained Tl:Pb:Hf:S ratios were homogeneous, but a more detailed analysis was inhibited by the strong overlaps of the Tl ($L\alpha$: 2.267 keV), Pb ($L\alpha$: 2.342 keV), and S ($K\alpha$: 2.307 keV) peaks.

Single-Crystal Structure Determinations. Suitable, platelike single crystals were obtained from the respective bulk sample for the single-crystal X-ray diffraction analysis. The data were collected at room temperature using a Bruker AXS Smart Apex (Tl_2PbZrS_4 and $Tl_2PbZrSe_4$), a Bruker AXS Kappa Apex II ($Tl_2PbHfSe_4$), and a Stoe IPDS 2 diffractometer (Tl_2PbHfS_4), all with Mo-Kα radiation. Lorentz and polarization corrections were applied, and the absorption corrections were based on fitting a function to the empirical transmission surface as sampled by multiple equivalent measurements. SAINT,[20] X-AREA, and SHELXTL[21] packages were used for the data reduction and structure refinement.

These compounds crystallize in the monoclinic system with the space group $C2/c$, in agreement with the systematic absences. Aside from the problem of differentiating between Tl and Pb sites, discussed in the Results and Discussion section of this Article, all refinements were straightforward. Afterward, the ADDSYMM program within the PLATON package was used to check for any missed symmetry.[22] The

dx.doi.org/10.1021/ic4025316 | Inorg. Chem. 2013, 52, 13869−13874

crystallographic data obtained from the four single-crystal refinements are listed in Table 1, and the atomic positions and equivalent displacement parameters are listed in Table 2.

Electronic Structure Calculations. We used the WIEN2k package for electronic structure calculations, which employs the full-potential linearized augmented plane-wave (FP-LAPW) method within density functional theory (DFT).[23,24] The generalized gradient approximation (GGA) from Perdew, Burke, and Ernzerhof was used for exchange and correlation energies.[25] We employed the following muffin-tin radii (R_{MT}): 2.5 Bohr for Tl, Pb, and Zr/Hf, 2.35 Bohr for Se, and 2.23 Bohr for S. The product $R_{MT} \times K_{Max}$ was set to be 7. For the self-consistent energy calculations, 100 k points were selected with an improved tetrahedron method within the irreproducible wedge of the first Brillouin zone. The energy convergence was set to be 10^{-4} Ry for the self-consistency. The relativistic spin−orbit (SO) coupling effects for the heavy atoms, Tl, Pb, and Hf, were also considered via a second variational procedure within the WIEN2k package. In addition, we utilized the LMTO (linear muffin-tin orbitals) method with the atomic spheres approximation (ASA)[26,27] to calculate the band structure of Tl_2PbZrS_4 with the LMTO47c package. Therein, the density functional theory is applied with the local density approximation (LDA)[28] instead of the GGA functional.

Physical Property Measurements. The optical spectra of the four title compounds were obtained within the UV−vis−near-IR region by using a Shimadzu UV-3101 spectrophotometer via diffuse reflectance measurements (followed by Kubelka−Munk transformation) at ambient conditions. The ULVAC-RIKO ZEM-3 was used to determine the Seebeck coefficient and the electrical conductivity of a cold-pressed pellet of $Tl_2PbHfSe_4$ within the temperature range from 300 to 520 K in a helium atmosphere as described before.[29,30]

RESULTS AND DISCUSSION

Crystal Structures. The chalcogenides Tl_2PbMQ_4 with M = Zr and Hf, and Q = S and Se, formed via solid-state reactions, crystallize in the monoclinic crystal system and belong to a new structure type. An analogous compound of the lightest group 4 element, Ti, was not formed. However, Tl_2PbGeS_4 was structurally characterized before and has a different atomic arrangement (space group $P2_1/c$), containing isolated GeS_4 tetrahedra[31] instead of MQ_6 octahedra in Tl_2PbMQ_4. The layered structure of Tl_2PbZrS_4 is revealed in Figure 1. Along the a axis, S layers—stacked in the sequence ABCABC—alternate with metal atom layers, which, in turn, are composed of alternating Tl layers and mixed Pb/Zr layers.

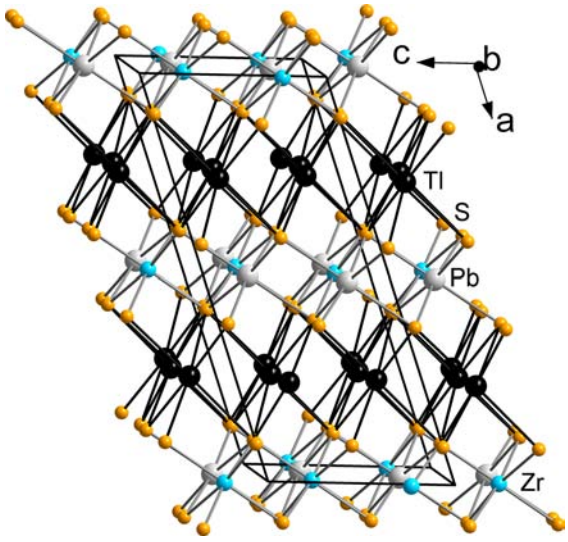

Figure 1. Layered crystal structure of Tl_2PbZrS_4.

All the metal atoms, viz. Tl, Zr, and Pb, are surrounded by six S atoms in more or less of an octahedral arrangement. TlS_6 octahedra are interconnected via edges to form a layer. Similarly, the PbS_6 and ZrS_6 octahedra are connected via edges. Each TlS_2 and $(Pb,Zr)S_2$ layer is thus topologically equivalent to the layers of the $CdCl_2$ type, but the octahedra are less regular. Reminiscent of the α-PbO_2 structure, the ZrS_6 octahedra can be viewed as zigzag chains that run along the c axis, as emphasized in Figure 2. Two such zigzag chains are

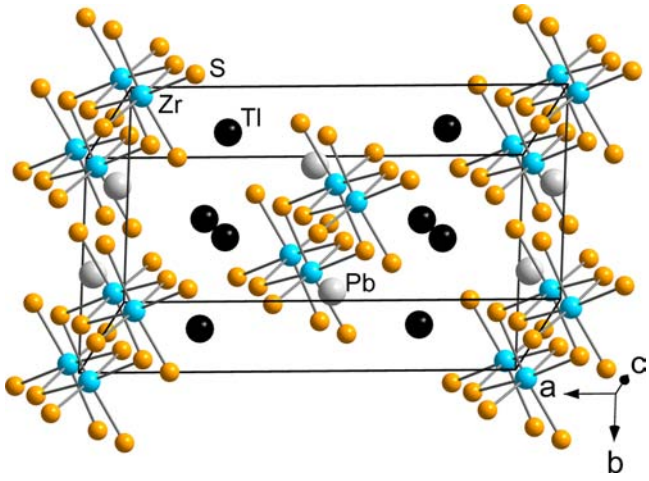

Figure 2. Chains of edge-shared ZrS_6 octahedra of Tl_2PbZrS_4.

separated by a similar zigzag chain formed from edge-shared PbS_6 octahedra. Similarly, ZrS_6 and PbS_6 polyhedra were also observed in $Tl_{18}Pb_2Zr_7S_{25}$,[19] the first quaternary material in this Tl−Pb−M−Q system.

The structure of Tl_2PbZrS_4 is also related to that of Tl_2ZrS_3.[15] Tl_2ZrS_3 adopts a layered structure with metal atoms occupying all octahedral voids created by hexagonal close-packed S atoms, with significant deviations from the ideal octahedral coordination of both the Tl and Zr atoms. Therein, all metal layers are symmetry-equivalent. ZrQ_6 octahedra share edges to form double chains that run along the c axis. In short, the Tl_2ZrS_3 structure can be viewed as a distorted variant of the α-$NaFeO_2$ type, a layered structure (based on ABAB packing) adopted by the thermoelectric tellurides $TlSbTe_2$ and $TlGdTe_2$.[32] On the other hand, the packing sequence of the S layers of Tl_2PbZrS_4 is ABCABC; therefore, the structure Tl_2PbZrS_4 may be viewed as a distorted variant of rock salt with different metal atom layers.

As listed in Table 3, the Zr−S distances in Tl_2PbZrS_4 vary from 2.53 to 2.63 Å, comparable to the corresponding ones in Tl_4ZrS_4 (2.52−2.66 Å) and ZrS_2 (2.56 Å). Three different Pb−S distances ranging from 2.91 to 2.95 Å exist in the PbS_6 octahedron, which are comparable to those observed in the binary PbS of 2.97 Å. The Tl atom forms bonds with S to assume a more distorted octahedral coordination, with larger bond lengths from 3.04 to 3.33 Å. We assume that there is no Tl/Pb mixing at the respective sites for Tl and Pb, as given in Table 2, noting that their multiplicities of 8 for Tl (8f site) and 4 for Pb (4e site) fit perfectly to the charge-balanced formula of $(Tl^+)_2Pb^{2+}M^{4+}(Q^{2-})_4$, and the high yields when using exactly twice as much Tl than Pb further support this argument. Pb^{2+} is the smaller ion with an ionic radius of 1.2 Å (Shannon,[33] 6-fold coordination) than six-coordinated Tl^+ (1.5 Å) and is likely to prefer the 4e site, sharing edges with ZrS_6 octahedra to form

dx.doi.org/10.1021/ic4025316 | Inorg. Chem. 2013, 52, 13869−13874

Table 3. Selected Metal−Q Distances [Å] of Tl_2PbMQ_4

metal	Q	count	Tl_2PbZrS_4	$Tl_2PbZrSe_4$	Tl_2PbHfS_4	$Tl_2PbHfSe_4$
Tl	Q1		3.109(4)	3.195(2)	3.101(3)	3.1986(5)
	Q1		3.243(3)	3.297(2)	3.257(3)	3.3106(5)
	Q1		3.266(4)	3.333(2)	3.273(3)	3.3492(6)
	Q2		3.043(4)	3.155(2)	3.026(3)	3.1471(5)
	Q2		3.106(3)	3.191(2)	3.109(3)	3.1929(5)
	Q2		3.325(4)	3.364(2)	3.331(3)	3.3749(5)
Pb	Q1	2×	2.906(3)	3.029(2)	2.921(3)	3.0317(5)
	Q2	2×	2.935(3)	3.030(2)	2.938(3)	3.0347(5)
	Q2	2×	2.952(4)	3.038(1)	2.965(3)	3.0391(5)
M	Q1	2×	2.589(3)	2.710(1)	2.568(3)	2.6894(5)
	Q1	2×	2.632(4)	2.753(3)	2.603(3)	2.7296(5)
	Q2	2×	2.531(4)	2.666(2)	2.524(3)	2.6804(5)

$(Pb/Zr)S_6$ layers. Thus, the Tl^+−S distance is commonly larger than the Pb^{2+}−S distance, as observed in binary Tl_2S (3.34 Å) and PbS (2.97 Å), respectively.

A common method to distinguish between differently charged cations is a calculation of the so-called bond-valence sums: the bond valences, v_{ij}, equal to $v_{ij} = \exp[(R_{ij} - d_{ij})/0.37$ Å], with d_{ij} being the here-observed distance between the two atoms *i* and *j*, and R_{ij} the respective expected value.[34] Using the Tl−S distance of 2.63 Å as R_{ij}, we calculated 1.4 and 2.7 for the sites identified as Tl and Pb, respectively, and 1.1 and 2.1 with the Pb−S distance of 2.55 Å as R_{ij}. Thus, this method also confirms that Pb as the 2+ cation should prefer this 4e site (identified as Pb).

The lack of strong homonuclear bonds suggests that all atoms could be assigned their most common oxidation state, as was also observed in $Tl_{18}Pb_2M_7Q_{25}$. Thus, an overall charge-balanced formula $(Tl^+)_2Pb^{2+}M^{4+}(Q^{2-})_4$ can be postulated with all atoms in a closed-shell configuration, which suggests semiconducting behavior.

Electronic Structures. The calculated DOS curves (without spin−orbit contribution) for the three materials Tl_2PbZrS_4, $Tl_2PbZrSe_4$, and $Tl_2PbHfSe_4$ are shown in Figure 3. All of these materials are semiconductors satisfying the charge-balanced formula suggested in the preceding section. In each case, the valence band is extended down to about −5 eV, consisting mostly of S/Se p states, while the lower part of the conduction band comprises metal d states along with the S/Se states due to covalent mixing. The sulfide, Tl_2PbZrS_4, was calculated to have a larger band gap (0.97 eV) than the corresponding selenides, $Tl_2PbZrSe_4$ (0.65 eV) and $Tl_2PbHfSe_4$ (0.63 eV). The decreasing trend in band gaps as we move from sulfides to selenides, also observed in $Tl_{18}Pb_2M_7Q_{25}$, is due to the higher electronegativity of S, as a result of which the S p orbitals occur at lower energies than the Se p orbitals.

Relativistic spin−orbit (SO) interactions can be important in these compounds because of the presence of heavy elements, such as Tl, Pb, and Hf, as demonstrated in the heavy metal containing thermoelectrics Tl_9SbTe_6[35] and $CsBi_4Te_6$.[36] For instance, the band gaps with and without SO effects in $CsBi_4Te_6$ were calculated to be around 0.04 and 0.4 eV, respectively, whereas the optical absorption edge was found to be around 0.1 eV.[37,38] Comparably, the calculated band gaps decreased in both Tl_2PbZrS_4 and $Tl_2PbHfSe_4$ after applying the SO correction from 0.97 and 0.63 eV to 0.65 and 0.35 eV, respectively, while valence bands dominated by the chalcogen p states barely changed (Figure 4). An extension of the energy range for the DOS of Tl_2PbZrS_4 (available as Supporting Information) reveals that the Tl s and Pb s states dominate lower-lying peaks around −6 and −8 eV, respectively.

Physical Properties. The results of the optical spectroscopy measurements are revealed in Figure 5. The absorption edges of both selenides occur around 1.2 eV, and of the sulfides around 1.5 eV for Tl_2PbZrS_4 and 1.6 eV for Tl_2PbHfS_4. These values are correlated with the direct band gaps, noting that the above calculated, smaller gaps were indirect, going from the Z point to the Γ point, i.e., from $c^*/2$ to the origin of the first Brillouin zone.

The thermoelectric power and electrical conductivity for the sample with the smallest calculated band gap, namely, $Tl_2PbHfSe_4$, were measured in the temperature range of 300−520 K on a cold-pressed pellet (Figure 6). This yielded large positive Seebeck coefficient values, increasing with increasing temperature, i.e., from S = +190 μV K^{-1} at room

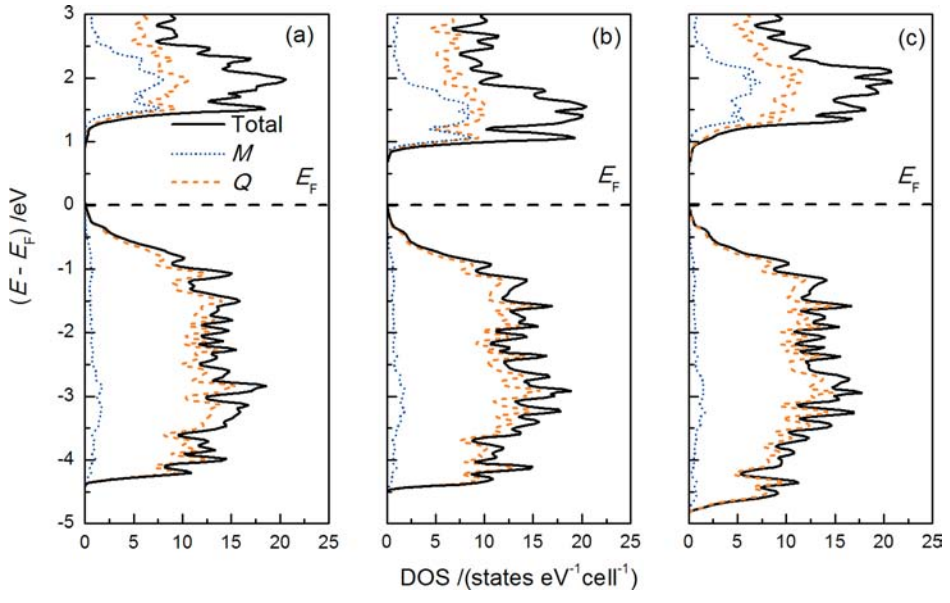

Figure 3. Density of states without spin−orbit contributions of (a) Tl_2PbZrS_4 (left), (b) $Tl_2PbZrSe_4$ (center), and (c) $Tl_2PbHfSe_4$ (right).

dx.doi.org/10.1021/ic4025316 | Inorg. Chem. 2013, 52, 13869−13874

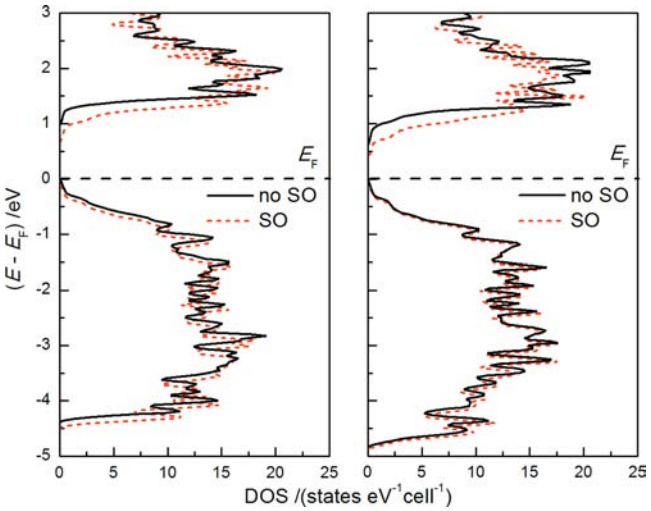

Figure 4. Density of states with and without SO contributions of Tl_2PbZrS_4 (left) and $Tl_2PbHfSe_4$ (right).

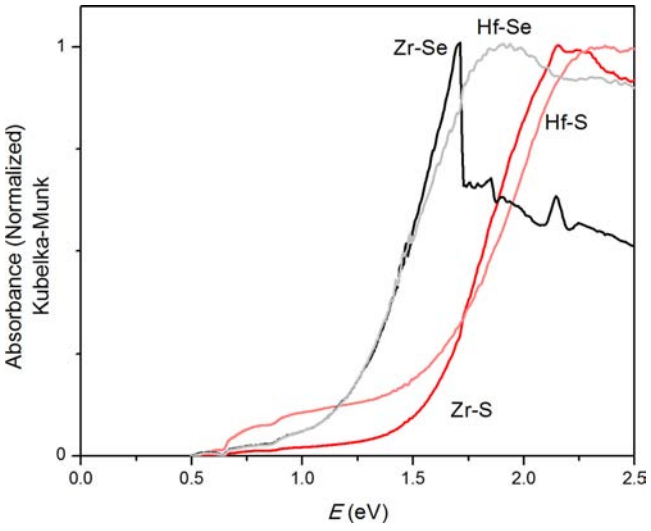

Figure 5. Optical absorbance spectra of Tl_2PbZrS_4 (denoted Zr-S), Tl_2PbHfS_4 (denoted Hf-S), $Tl_2PbZrSe_4$ (denoted Zr-Se), and $Tl_2PbHfSe_4$ (denoted Hf-Se).

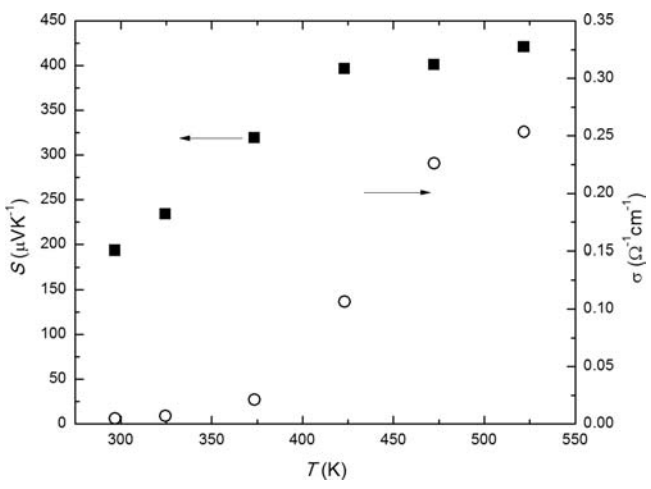

Figure 6. Seebeck coefficient and electrical conductivity of $Tl_2PbHfSe_4$.

temperature to +420 μV K^{-1} at 520 K. These values lie mostly between those measured for $Tl_{18}Pb_2Ti_7Se_{25}$ and $Tl_{18}Pb_2Zr_7Se_{25}$, and the positive sign is indicative for p-type conduction, as is often observed in undoped chalcogenides. The electrical conductivity values increased from σ = 0.005 Ω^{-1} cm^{-1} at 300 K to 0.25 Ω^{-1} cm^{-1} at 520 K, which is in the normal range for undoped semiconductors. For thermoelectrics, however, values in excess of 500 Ω^{-1} cm^{-1} are required. Moreover, the power factor values, P.F. = $S^2\sigma$, increased from only 1.7 × 10^{-4} μW cm^{-1} K^{-2} at 300 K to 4.5 × 10^{-2} μW cm^{-1} K^{-2} at 520 K, while advanced thermoelectrics exhibit P.F. values of several μW cm^{-1} K^{-2}. The room-temperature electrical conductivity of the sulfide sample, Tl_2PbHfS_4, was found to be only of the order of 10^{-6} Ω^{-1} cm^{-1}, which restricted further studies on its intrinsic physical properties.

CONCLUSIONS

This contribution introduced the second family of new materials—Tl_2PbMQ_4—in the quaternary Tl−Pb−*M*−Q system after the discovery of $Tl_{18}Pb_2M_7Q_{25}$ (with *M* = Zr, Hf and Q = S, Se). Like the representatives of $Tl_{18}Pb_2M_7Q_{25}$, the sulfides and selenides Tl_2PbMQ_4 are isostructural, whereas we were unable to prepare tellurides with those elemental ratios. The structure of Tl_2PbMQ_4 consists of densely packed Q layers, with the octahedral holes in every other layer being filled with Tl, alternating with Pb and Zr/Hf in octahedral holes. As such, there is a strong resemblance of this new structure type to the structures of $TlSbTe_2$ and $TlBiTe_2$ (α-$NaFeO_2$ type) as well as to the related chalcogenides Tl_2MQ_3.

All of these materials are semiconducting, with calculated indirect band gaps below 1 eV, and optical gaps of 1.2−1.6 eV. Thusly, several criteria for good thermoelectric performance are met, namely, heavy elements, complex crystal structures, covalent bonding, and narrow gaps (at least for the selenides). While the performance of the undoped samples is poor because of the low electrical conductivity, attempts will be made to enhance the carrier concentration and thusly the electrical conductivity via doping, e.g., by altering the Tl/Pb ratio and by introducing small amounts of Nb, Ta, or Mo on the *M* sites.

ASSOCIATED CONTENT

Supporting Information

Four experimental powder diagrams, four crystallographic information files combined into one file (CIF), the DOS of Tl_2PbZrS_4 highlighting the Tl and Pb states, and the band structure and DOS of Tl_2PbZrS_4 calculated with the LMTO approach. This material is available free of charge via the Internet at http://pubs.acs.org.

AUTHOR INFORMATION

Corresponding Author

*E-mail: kleinke@uwaterloo.ca.

Notes

The authors declare no competing financial interest.

ACKNOWLEDGMENTS

Financial support from the Natural Sciences and Engineering Research Council is appreciated.

REFERENCES

(1) Rowe, D. M. *Thermoelectrics Handbook: Macro to Nano*; CRC Press, Taylor & Francis Group: Boca Raton, FL, 2006.

(2) Kleinke, H. *Chem. Mater.* **2010**, *22*, 604−611.
(3) Toberer, E. S.; May, A. F.; Snyder, G. J. *Chem. Mater.* **2010**, *22*, 624−634.
(4) Kanatzidis, M. G. *Chem. Mater.* **2010**, *22*, 648−659.
(5) Hsu, K. F.; Loo, S.; Guo, F.; Chen, W.; Dyck, J. S.; Uher, C.; Hogan, T.; Polychroniadis, E. K.; Kanatzidis, M. G. *Science* **2004**, *303*, 818−821.
(6) Quarez, E.; Hsu, K.-F.; Pcionek, R.; Frangis, N.; Polychroniadis, E. K.; Kanatzidis, M. G. *J. Am. Chem. Soc.* **2005**, *127*, 9177−9190.
(7) Karkamkar, A. J.; Kanatzidis, M. G. *J. Am. Chem. Soc.* **2006**, *128*, 6002−6003.
(8) Biswas, K.; He, J.; Blum, I. D.; Wu, C.-I.; Hogan, T. P.; Seidman, D. N.; Dravid, V. P.; Kanatzidis, M. G. *Nature* **2012**, *489*, 414−418.
(9) Guo, Q.; Chan, M.; Kuropatwa, B. A.; Kleinke, H. *Chem. Mater.* **2013**, *25*, 4097−4104.
(10) Wölfing, B.; Kloc, C.; Teubner, J.; Bucher, E. *Phys. Rev. Lett.* **2001**, *86*, 4350−4353.
(11) Kuropatwa, B. A.; Assoud, A.; Kleinke, H. *J. Alloys Compd.* **2011**, *509*, 6768−6772.
(12) Kurosaki, K.; Kosuga, A.; Yamanaka, S. *J. Alloys Compd.* **2003**, *351*, 279−282.
(13) Kurosaki, K.; Uneda, H.; Muta, H.; Yamanaka, S. *J. Alloys Compd.* **2004**, *376*, 43−48.
(14) Kurosaki, K.; Kosuga, A.; Muta, H.; Uno, M.; Yamanaka, S. *Appl. Phys. Lett.* **2005**, *87*, 061919.
(15) Sankar, C. R.; Kuropatwa, B. A.; Assoud, A.; Kleinke, H. *Dalton Trans.* **2012**, *41*, 9646−9650.
(16) Sankar, C. R.; Guch, M.; Assoud, A.; Kleinke, H. *Chem. Mater.* **2011**, *23*, 3886−3891.
(17) Sankar, C. R.; Bangarigadu-Sanasy, S.; Assoud, A.; Kleinke, H. *Inorg. Chem.* **2011**, *50*, 245−249.
(18) Sankar, C. R.; Bangarigadu-Sanasy, S.; Assoud, A.; Kleinke, H. *J. Mater. Chem.* **2010**, *20*, 7485−7490.
(19) Sankar, C. R.; Becker, A.; Assoud, A.; Kleinke, H. *Inorg. Chem.* **2013**, *52*, 1895−1900.
(20) *M86-Exx078 APEX2 User Manual*; Bruker AXS Inc.: Madison, WI, 2006.
(21) Sheldrick, G. M. *Acta Crystallogr., Sect. A* **2008**, *64*, 112−122.
(22) Spek, A. L. *J. Appl. Crystallogr.* **2003**, *36*, 7−13.
(23) Blaha, P.; Schwarz, K.; Madsen, G. K. H.; Kvasnicka, D.; Luitz, J. *WIEN2k: An Augmented Plane Wave + Local Orbitals Program for Calculating Crystal Properties*; Techn. Universität Wien: Wien, Austria, 2001.
(24) Schwarz, K. *J. Solid State Chem.* **2003**, *176*, 319−328.
(25) Perdew, J. P.; Burke, K.; Ernzerhof, M. *Phys. Rev. Lett.* **1996**, *77*, 3865−3868.
(26) Andersen, O. K. *Phys. Rev. B* **1975**, *12*, 3060−3083.
(27) Skriver, H. L. *The LMTO Method*; Springer: Berlin, Germany, 1984.
(28) Hedin, L.; Lundqvist, B. I. *J. Phys. C: Solid State Phys.* **1971**, *4*, 2064−2083.
(29) Guch, M.; Sankar, C. R.; Salvador, J. R.; Meisner, G. P.; Kleinke, H. *J. Appl. Phys.* **2012**, *111*, 063706.
(30) Wang, H.; Porter, W. D.; Böttner, H.; König, J.; Chen, L.; Bai, S.; Tritt, T. M.; Mayolett, A.; Senawiratne, J.; Smith, C.; Harris, F.; Gilbert, P.; Sharp, J. W.; Lo, J.; Kleinke, H.; Kiss, L. I. *J. Electron. Mater.* **2013**, *42*, 654−664.
(31) Eulenberger, G. *Z. Naturforsch., B* **1980**, *35*, 335−339.
(32) Sankar, C. R.; Bangarigadu-Sanasy, S.; Kleinke, H. *J. Electron. Mater.* **2012**, *41*, 1662−1666.
(33) Shannon, R. D. *Acta Crystallogr.* **1976**, *A32*, 751−767.
(34) Brese, N. E.; O'Keeffe, M. *Acta Crystallogr., Sect. B* **1991**, *47*, 192−197.
(35) Tao, X.; Jund, P.; Viennois, R.; Tédenac, J.-C. *J. Phys. Chem. A* **2011**, *115*, 8761−8766.
(36) Chung, D.-Y.; Hogan, T.; Brazis, P.; Rocci-Lane, M.; Kannewurf, C.; Bastea, M.; Uher, C.; Kanatzidis, M. G. *Science* **2000**, *287*, 1024−1027.
(37) Larson, P.; Mahanti, S. D.; Chung, D.-Y.; Kanatzidis, M. G. *Phys. Rev. B* **2002**, *65*, 045205.
(38) Chung, D.-Y.; Hogan, T. P.; Rocci-Lane, M.; Brazis, P.; Ireland, J. R.; Kannewurf, C. R.; Bastea, M.; Uher, C.; Kanatzidis, M. G. *J. Am. Chem. Soc.* **2004**, *126*, 6414−6428.